Single-Molecule Atomic Force Microscopy Force Spectroscopy Study of Aβ-40 Interactions

Bo-Hyun Kim,[†] Nicholas Y. Palermo,[‡] Sándor Lovas,[‡] Tatiana Zaikova,[§] John F. W. Keana,[§] and Yuri L. Lyubchenko*,[†]

[†]Department of Pharmaceutical Sciences, University of Nebraska Medical Center, 986025 Nebraska Medical Center, Omaha, Nebraska 68198, United States

[‡]Department of Biomedical Science, Creighton University, Omaha, Nebraska 68178, United States

[§]Department of Chemistry, 1253, University of Oregon, Eugene, Oregon 97403-1253, United States

Ⓢ *Supporting Information*

ABSTRACT: Misfolding and aggregation of amyloid β-40 (Aβ-40) peptide play key roles in the development of Alzheimer's disease (AD). However, very little is known about the molecular mechanisms underlying these molecular processes. We developed a novel experimental approach that can directly probe aggregation-prone states of proteins and their interactions. In this approach, the proteins are anchored to the surface of the atomic force microscopy substrate (mica) and the probe, and the interaction between anchored molecules is measured in the approach—retraction cycles. We used dynamic force spectroscopy (DFS) to measure the stability of transiently formed dimers. One of the major findings from DFS analysis of α-synuclein (α-Syn) is that dimeric complexes formed by misfolded α-Syn protein are very stable and dissociate over a range of seconds. This differs markedly from the dynamics of monomers, which occurs on a microsecond to nanosecond time scale. Here we applied the same approach to quantitatively characterize interactions of Aβ-40 peptides over a broad range of pH values. These studies showed that misfolded dimers are characterized by lifetimes in the range of seconds. This value depends on pH and varies between 2.7 s for pH 2.7 and 0.1 s for pH 7, indicating that the aggregation properties of Aβ-40 are modulated by the environmental conditions. The analysis of the contour lengths revealed the existence of various pathways for dimer dissociation, suggesting that dimers with different conformations are formed. These structural variations result in different aggregation pathways, leading to different types of oligomers and higher-order aggregates, including fibrils.
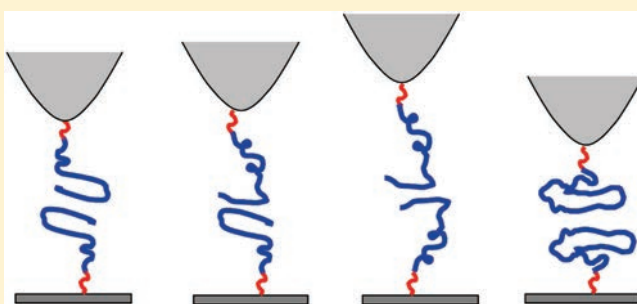
Protein misfolding and self-assembly into various morphologic aggregates are widespread phenomena in the development of various neurodegenerative disorders such as Alzheimer's and Parkinson's diseases.[1,2] The aggregation properties of amyloid β (Aβ) peptide, a key protein for Alzheimer's disease, have been studied using various methods.[3−7] The current model for amyloidogenic peptides dissects the aggregation kinetics into two main phases. Historically, self-assembly kinetics were observed initially in the earlier work of Hofrichter et al.,[8] in which the gelation phenomenon of purified deoxyhemoglobin was investigated. The authors proposed a model that dissected the growth kinetics of fibrils into two phases. The first phase is the nucleation process. During this phase, a critical oligomer of a particular size (nucleus) is formed. The nucleus undergoes a thermodynamically favorable elongation process in which monomers are added via consecutive steps. This model, applied to the aggregation of deoxyhemoglobin, suggested the size of the nucleus to be as large as 30 monomeric units.[8] Jarrett and Lansbury applied this model to analyze the aggregation of amyloids that followed a similar kinetic profile.[9] It was recently shown that growth of amyloid plaques in vivo follows the same

model.[10] Both in vivo and in vitro studies indicate a considerably long lag period during which stable nuclei form. This period is considered a key step in the process of amyloid growth. However, a number of important questions arise. What are these nuclei? How large are they? How long do they live? Answering these questions is important, as soluble oligomeric assemblies of Aβ rather than fibrils are neurotoxic[11] and the dimer is the smallest synaptotoxic species.[12,13]

Progress has been made recently in understanding the early stages of aggregation and misfolding of proteins. The ionization mass spectrometry (ISI-MS) method was developed to characterize oligomeric species of Aβ peptides.[3] This ISI-MS using study shows that oligomerization of Aβ-40 and that of Aβ-42 follow two different aggregation pathways with tetramers and hexamers as potential nuclei. Importantly, in both cases, dimers are the building blocks. Spectroscopic analysis of covalently cross-linked Aβ-42 oligomers[4,14] showed that changes in the

structure of Aβ-42 occur rapidly in the transition from monomer to dimer and then proceed gradually for higher-order oligomers. A combined approach utilizing several methods to study entire aggregation kinetics has been recently proposed.[15] The proposed kinetic model suggests that the β-LGA monomers are converted into dimers and tetramers in the early stages of aggregation, and these species, primarily tetramers, constitute a reservoir of intermediates used for the later stages of the aggregation process. A common feature exists in the studies performed on two different types of amyloidogenic proteins, the conversion of monomers into dimers, followed by their assembly into tetramers. No trimers are detected in either study. These findings suggest that dimers may contain a property that makes their accumulation preferable compared to the use of monomers as building materials for the growth of oligomers. Recently, a novel approach to characterizing misfolded states and dimeric forms of the amyloidogenic proteins was proposed.[16,17] In this technique, the interaction between the proteins is measured by AFM force spectroscopy with significant rupture forces, suggesting that misfolded proteins form dimeric states. This approach was tested initially with the use of three different proteins, α-synuclein, lysozyme, and amyloid β peptide.[16] Further improvement of the protein immobilization methodology made it possible to provide the characterization of misfolded dimers at the single-molecule level.[18] The dynamic force spectroscopy (DFS) approach was used to characterize interactions of α-synuclein (α-Syn).[19,20] One of the major findings from DFS analysis is that dimeric complexes formed by misfolded α-Syn protein are very stable and dissociate over a range of seconds. This differs markedly from the dynamics of monomers, which occurs on a microsecond to nanosecond time scale. This finding, along with other recent publications,[3,15] suggests that dimerization is the key step in the self-assembly process.

Here, we have applied the AFM force spectroscopy methodology to test whether the interaction of the Aβ-40 peptide follows the same model. We used DFS to measure the stability of transiently formed Aβ-40 dimers. The aggregation properties of Aβ-40 depend on structural properties of Aβ-40 that are modulated by the environmental conditions.[21−23] Therefore, we performed DFS analysis over a range of pH values. These experiments showed that like α-Syn protein, Aβ-40 forms dimers with lifetimes in the range of seconds. The analysis of the contour lengths revealed variations in the interactions of Aβ-40. This suggests that dimers with different conformations are formed, which we propose are capable of leading to diverse aggregation pathways of Aβ-40.

■ MATERIALS AND METHODS

Synthesis of Cysteine-Modified Aβ-40. The procedure is described in detail in the Supporting Information. Briefly, the cysteine-modified N-terminus of Aβ-40 (Cys-Aβ-40) was synthesized on a CEM Liberty microwave peptide synthesizer using a Val-HMPB Chemmatrix resin. We cleaved the synthesized peptide from the resin by stirring the peptide resin with a TFA/thioanisole/phenol/H$_2$O/dimethyl sulfide/ethanedithiol/triisopropylsilane mixture. After cleavage, the peptide was dissolved in 100 μL of TFA, which was then diluted with 100 mL of H$_2$O and injected into a Vydac C4 semipreparative RP-HPLC column for purification (see the details in the Supporting Information). The purified peptide was characterized by ESI mass spectrometry

and sodium dodecyl sulfate−polyacrylamide gel electrophoresis (Figure S1 of the Supporting Information).

Silatrane-Derivatized Tetrahedrally Shaped (T-silatrane) Molecule. The nanoscale tetrahedrally shaped tripodal silatrane incorporating a chemically reactive terminal maleimide group (Figure S2 of the Supporting Information) has been synthesized as described in the Supporting Information and used without extra purification.

Tip and Mica Surface Modification. The general process for the cleaning and modification of the tip and mica surfaces was similar to the previously reported protocol.[19,20] Briefly, tips (MLCT, Veeco, Santa Barbara, CA) were cleaned with ethylene alcohol followed by UV treatment for 30 min and modified with maleimide polyethylene glycol silatrane (MAS).[18] The freshly cleaved mica surface was modified with 1-(3-aminopropyl)silatrane (APS), and then N-hydroxysuccinimide-polyethylene glycol-maleimide (NHS-PEG-MAL) (MW of 3400 g/mol, Laysan Bio Inc., Arab, AL) was coupled to the amine group of APS in DMSO in a dry chamber for 3 h. Both functionalization protocols yielded surfaces terminated with maleimide headgroups capable of covalent bonding with Aβ-40 at the N-terminal cysteine. To accomplish this step, the functionalized tip and mica were incubated with an ∼20 nM solution of Aβ-40 diluted in HEPES buffer (pH 7) for 1 h and then gently rinsed with the dilution buffer and NaCO$_3$/NaHCO$_2$ (pH 10) buffer. Prepared tips and mica were kept in HEPES buffer until needed.

Modification of the Si-Wafer with Tetrahedrally Shaped Tripodal Silatrane [T-shaped (see Figure S2 of the Supporting Information)]. N-Type Si-wafer (NOVA electronic materials, Flower Mound, TX) was cleaned using the standard cleaning process.[24] Before the standard cleaning process, the wafer was cleaned with piranha solution (3:1 sulfuric acid/hydrogen peroxide mixture) for 30 min and then rinsed with DI water several times. Precleaned Si-wafer was immersed in SC1 cleaner (5:1:1 water/ammonium hydroxide/hydrogen peroxide mixture) and then SC2 cleaner (6:1:1 water/hydrogen chloride/hydrogen peroxide mixture) at ∼70 °C for 15 min for each step. After each cleaning step, wafer was washed with DI water. The cleaned Si-wafer surface was modified with T-shaped silatrane. The molecule was dissolved at a concentration of 1 mg/mL in DMSO as a stock solution and then diluted in a DMSO/H$_2$O mixture (80:20) before use. The cleaned wafer (1 cm × 1 cm) was covered with 30 μL of a diluted T-shaped molecule (167 μM) and was kept in a closed chamber overnight. After being modified, the wafer was rinsed several times using DMSO and then DI water. On the modified Si-wafer surface, Aβ protein was immobilized through the process described above.

The working buffer solutions were prepared at five different pHs: pH 2.7 (20 mM glycine-HCl), pH 3.7 (10 mM sodium acetate), pH 5 (10 mM sodium acetate), pH 7 (20 mM HEPES), and pH 9.8 (100 mM sodium carbonate and sodium bicarbonate). All buffers were adjusted to an ionic strength of 150 mM with NaCl.

Single-Molecule Force Spectroscopy. The force−distance curve (FDC) of Aβ was measured at four different pH values (2.7, 3.7, 5, and 7) with a MFP3D AFM instrument (Asylum Research, Santa Barbara, CA) at room temperature. The spring constant of tips (MLCT, Veeco) was 30−60 pN/nm, which was calibrated with the thermal noise analysis method. We applied a 100 pN force (trigger) at the contact. At high retracting velocities (≥1 μm/s), the tip was kept at the surface for 0.3 s (dwell time). The retracting velocity varied from 50 nm/s to 3 μm/s with
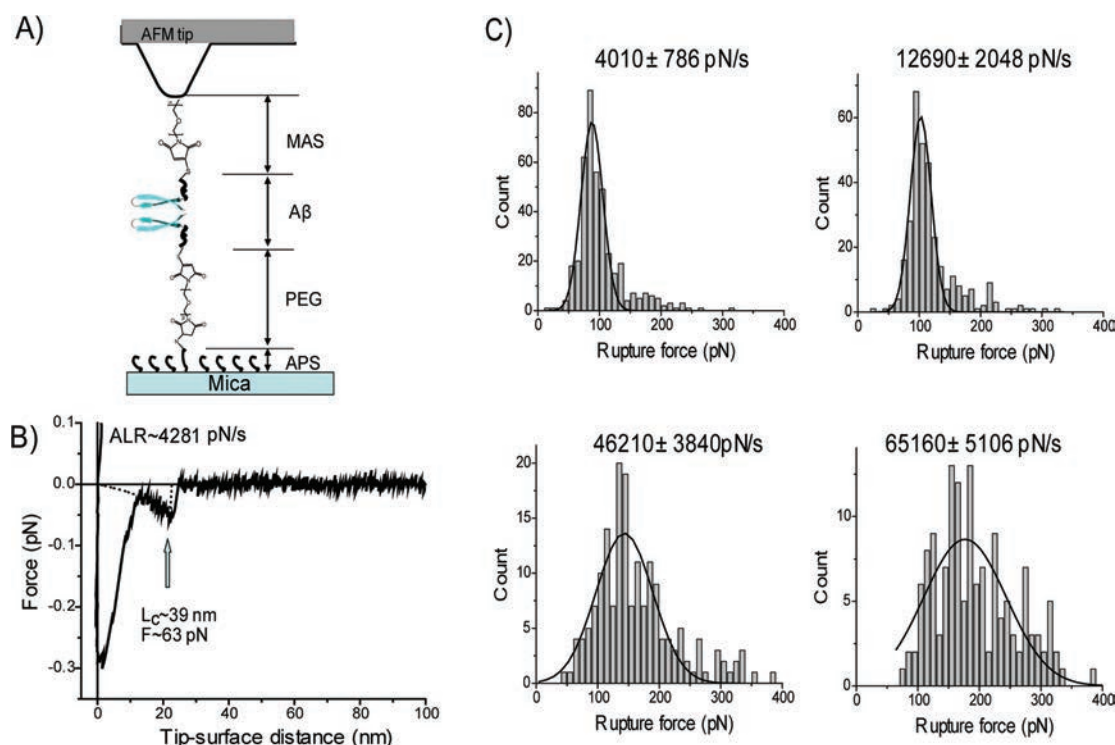
Figure 1. (A) Schematic experimental system of SMFS. The AFM tip and mica surface were functionalized with MAS and Aβ-40 and with APS, PEG, and Aβ-40, respectively. In the schematic, Aβs are shown as β-hairpin structures in dimeric form. (B) Representative force−distance curve measured at pH 5 with an apparent loading rate (ALR) of 4280 pN/s. (C) Histograms of the rupture force distribution measured at pH 5 at ALRs of 4000, 12690, 46210, and 65160 pN/s. The most probable rupture forces (F_r) for each loading rate were ∼88, ∼102, ∼143, and ∼177 pN, respectively, which were calculated by Gaussian fitting.

seven or eight discrete steps corresponding to an apparent loading rate of 1000−200000 pN/s. FDCs were collected more than 2000 times per each retracting velocity on five to seven different batches. The selected FDCs were analyzed using the wormlike chain (WLC) model with Igor Pro version 6.01.

Data Analysis. The contour length analysis was performed with the WLC model for flexible linkers[25] as described in previous publications.[18,19,26,27] These papers also describe specifics for DFS methods used in this paper. While the individual FDCs were fitted to the WLC model [$F_p = 1/4k_BT(1 - x/L)^{-2} - 1/4 + x/L$, where F is rupture force, p is persistence length, k_BT is thermal energy, and L is contour length], the persistence length was allowed to be varied for the best fitting curve and evaluated as a variable parameter along with contour length. The WLC fitting procedure as a part of the software was provided by the MFP 3D manufacturer (Asylum Research). An example of such a fit is shown in Figure S6A of the Supporting Information. The persistence length was an adjustable parameter with a mean value 0.16 ± 0.1 nm in the distribution histogram (Figure S6B of the Supporting Information). On the basis of the parameters of the DFS result, the conceptual simplified energy landscape was constructed on the reaction coordinate.[28]

■ RESULTS

Experimental Design. Figure 1A provides the schematics for our experimental approach. We used a variant of the Aβ-40 peptide with cysteine at the N-terminus to specifically immobilize proteins at the tip and the mica surface functionalized by maleimide using appropriate linkers.[18−20,27] This immobilization

approach was selected because the N-terminus of Aβ-40 is not involved in fibril formation.[6,29,30] Aβ-40 was covalently attached to the maleimide-terminated surface at its N-terminal cysteine, and the interaction between the protein molecules was measured by multiple approach−retraction cycles. The cysteine sulfhydryl group was attached to the mica surface via a polyethylene glycol linker (PEG, 19−26 nm long). A shorter PEG spacer of maleimide silatrane (MAS) provided immobilization of Aβ-40 to the AFM tip using a one-step modification procedure.[18] A freshly prepared ∼20 nM working solution of peptide was used in each experiment, and 0.25 mM TCEP was added to minimize the dimerization of the peptide via S−S bond formation. Note that the concentration of the protein was more than 3 orders of magnitude less than the protein concentration used in the aggregation experiments in vitro. Under these conditions, we obtained a sparse distribution of the peptide on the surface minimizing the double-rupture events.[26]

Interactions between Aβ-40 at pH 5. A typical force−distance curve for the rupture events of the experiments performed at pH 5 is shown in Figure 1B. pH 5 corresponds to conditions at which Aβ-40 is mostly neutral (pI 5.4). The first large peak of the FDC corresponds to the short-range nonspecific interactions typically appearing in AFM force measurement experiments.[20,27] The second peak is separated from the initial peak by a specific distance, similar to prior studies.[19,20,26] This distance is defined primarily by the length of the flexible linkers and unstructured segments of the peptide. The peak shown in Figure 1B corresponds to a contour length L_c of ∼39 nm, which is in the range of expected values (Figure 1A and Table S1 of the Supporting Information). The force curves similar to the one in
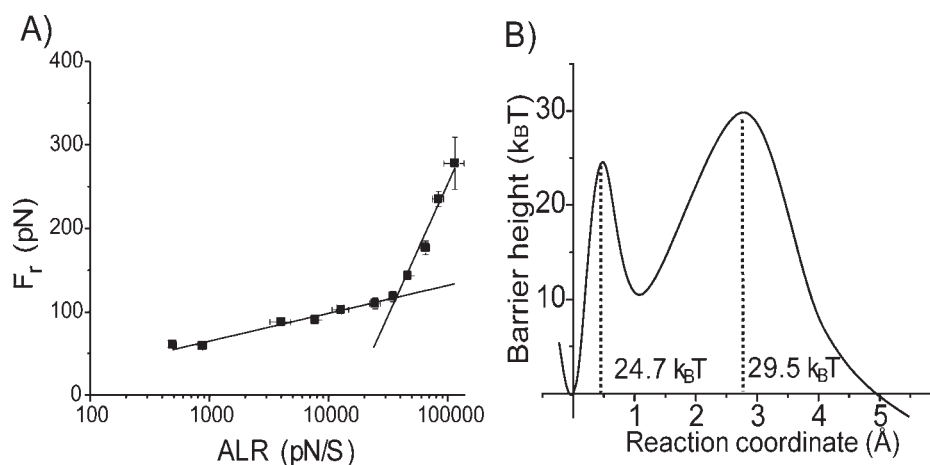
Figure 2. Results of dynamic force spectroscopy analysis at pH 5. (A) Dependence of F_r on the logarithm of ALR. The solid lines represent the best fits of data points in two regimes by Bell's model. (B) Profile of the energy landscape calculated from the DFS plot above. The parameters are listed in Table 1.

this figure were acquired by multiple probings over various positions of the tip over the surface. The DFS analysis required the system pulling with various rates. Therefore, the probing experiments were performed over a broad range of loading rates (0.1−100 nN/s). To generate the DFS spectrum, we collected more than 25000 force curves. The mean yield of the rupture events was 6.5%, and they all were analyzed. In the control experiments without peptides, nonspecific rupture events appeared at short contour lengths (<30 nm) and the forces were distributed over a broad range (from 20 pN to 1.5 nN). The yield of such an event was <1%. The most probable rupture force (F_r) for a selected pulling rate was calculated from the Gaussian fitting of the histograms of rupture force distribution (Figure 1C).

Figure 2A shows the plot of F_r obtained for different pulling rates versus the apparent loading rates on a logarithmic scale. Each data point was obtained by averaging over five independent experiments. The data set was approximated by the Bell−Evans model[31−33] with two straight lines indicating that there were two transient states for Aβ-40 dissociation under this condition. Two major parameters obtained from this plot, the intercept and the slope, were used to reconstruct the energy landscape profile for the dissociation of the dimer shown in Figure 2B. The first (inner barrier) and second (outer barrier) transient states correspond to the higher and the lower slopes in Figure 2A, respectively. The transient states for this process are located 0.3 and 2.6 Å from the ground state of the dimer. The inner barrier height ($\Delta G = 24.7k_BT$) and the dissociation lifetime ($\tau_{in} = 0.009$ s) were obtained from the off-rate constant (K_{off}). A similar analysis for the outer barrier provided the following numbers: $\Delta G = 29.5k_BT$, and $\tau_{out} = 1.13$ s.

Effect of pH on the Aβ-40 Interactions. Similar DFS analyses were performed at pH 7, 3.7, and 2.7. The results are shown in DFS plots and landscape energy profiles in Figure 3. The DFS plot for pH 7 (Figure 3A) is represented by a single line suggesting that there is only one transient state. The corresponding energy landscape profile is shown to the right (Figure 3B). Figure 3C shows the DFS result obtained at pH 3.7. This plot has two slopes, and the corresponding profile of the energy landscape with two barriers is shown in Figure 3D. Note the proximity of the inner barrier to the ground state of the dimer. The results of the DFS analysis for acidic conditions, pH 2.7, are shown in

panels E and F of Figure 3. The two-slope plot (Figure 3E) generates the profile of the energy landscape with two barriers (Figure 3F). Note a relatively distant position of the outer barrier compared with other profiles. The values for the off-rate constants, lifetimes, and positions of the barriers characterizing the Aβ-40 dissociation processes are summarized in Table 1. The lifetimes corresponding to the dimer dissociation (outer barrier height) vary between 2.7 s for pH 2.7 and 0.1 s for pH 7. The lifetimes for the inner barriers of pH 2.7, 3.7, and 5 are in the range of 10 ms, indicating that the transient state of the inner barrier is ∼100 times more dynamic than that of the outer barrier.

Modes of Interaction in Aβ-40 Dimers. The force curves in the AFM force spectroscopy experiments, in addition to the rupture force values, provide another important value, the contour length L_c (Figure 1B). According to panels A and B of Figure 1, the contour length primarily comprises the length of the flexible linker and the N-terminal segment of the peptide not involved in dimer formation. Therefore, subtracting the lengths of the linkers from the experimentally measured contour length yields the length of the N-terminal segment of the peptide preceding the structured segment of Aβ-40 involved in the interpeptide interaction. We tested and applied this approach in our recent work on the localization of interacting segments in misfolded α-synuclein.[19,20]

Figure 4A shows a set of four force curves obtained at pH 5. These force curves have very close rupture force values (∼120 pN) but differ in the rupture position between ∼25 nm (L_0) and ∼45 nm (L_3). The contour lengths measured from hundreds of rupture events were collected and are shown as a histogram in Figure 4B. The contour lengths vary between 30 and 60 nm. Similar data were obtained for pH 2.7, 3.7, and 7, as shown in panels C−E of Figure 4, respectively. The histograms at each pH are broad, but the profiles are different. For example, the representative rupture events for pH 5 are those with lengths between 49 and 56 nm, whereas probing at pH 2.7 has the most representative lengths between 36 and 43 nm. The contribution of flexible linkers to the contour lengths is 26 ± 4 nm (Figure 1A) (see the Supporting Information). The error in this value is due to the heterogeneity of the PEG linker and rupture force. Subtracting this value from the total range of contour lengths yields a range from 8 to 38 nm, which represents the variability of
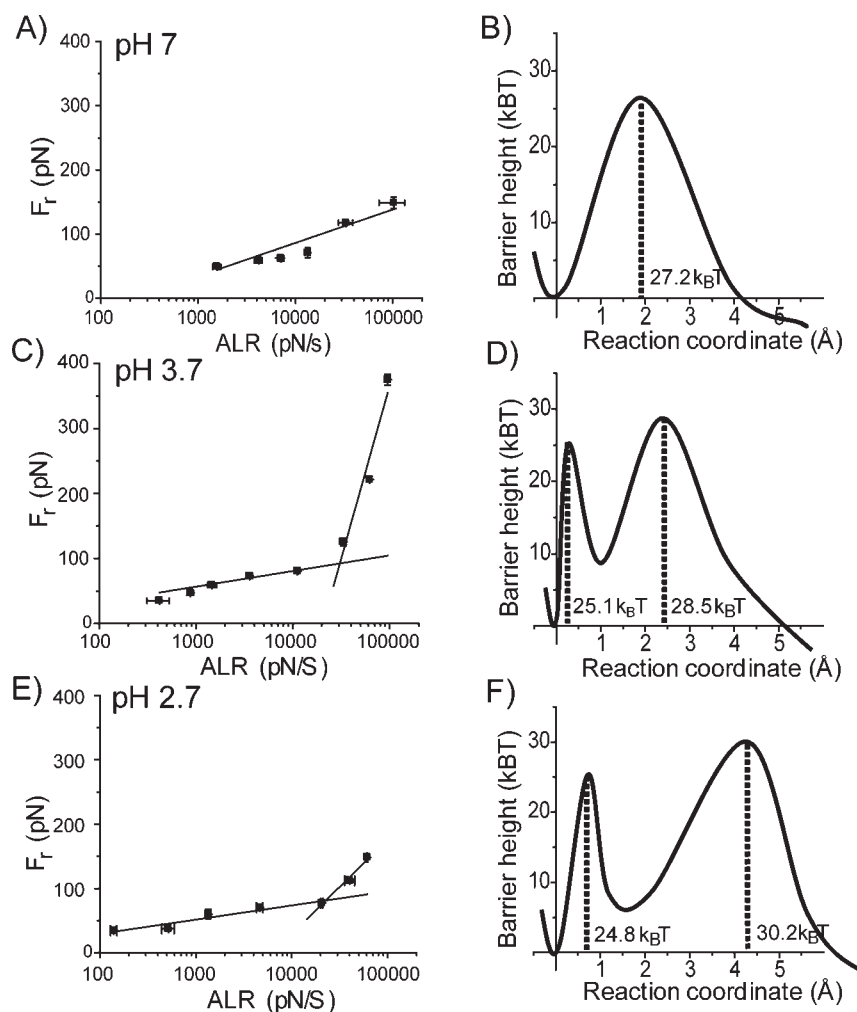
Figure 3. Results of the dynamic force spectroscopy analysis for different pH values. Each pair consists of the DFS plot and the corresponding profile of the energy landscape at pH 7 (A and B), pH 3.7 (C and D), and pH 2.7 (E and F). In the energy landscapes, the first valley is for the bound state, the second is for the intermediate, and the last is for the dissociation state of $A\beta$-40 dimers. The potential barrier heights were calculated using K_{off} (see the text) extracted from the linear fitting of Bell's model in the plot of F_r vs ln(ALR). All parameters used for energy landscapes are listed in Table 1.

Table 1. Characteristic Parameters of DFS Results[a]

pH	$X_{\beta1}$ (pm)	K_{off1} (s^{-1})	lifetime (s)	$X_{\beta2}$ (pm)	K_{off2} (s^{-1})	lifetime (ms)
2.7	427 ± 21	0.4 ± 0.2	2.7 ± 1.1	60 ± 10	104 ± 21	10 ± 2
3.7	244 ± 26	2.5 ± 0.8	0.4 ± 0.1	20 ± 6	78 ± 12	13 ± 2
5	265 ± 27	0.9 ± 0.2	1.1 ± 0.3	28 ± 5	114 ± 12	9 ± 1
7	182 ± 11	9.4 ± 1.5	0.1 ± 0.01			

[a] $X_{\beta1}$ and $X_{\beta2}$ are the outer and inner potential barrier locations and K_{off1} and K_{off2} the outer and inner dissociation ratios, respectively. The lifetime (τ) was calculated by $\tau \sim 1/K_{off}$ and the standard deviation (SD) was calculated from several data sets measured at each pH.

the N-terminal segment of the $A\beta$-40 peptide, including the dimeric structure length. Such broad variability suggests that the conformation of the peptide in the complexes is not constant; rather, $A\beta$-40 adopts a set of conformations. To confirm this assumption and to exclude the potential effect of the linkers, we performed similar probing experiments with the use of very short linkers. The major problem with the use of short linkers is the adhesion at small distances. To minimize this problem, we used

tetrahedrally shaped silatrane linkers (T-silatrane) with tripodal silatrane arms (Figure S2 of the Supporting Information). This molecule has three arms with silatrane end groups allowing the immobilization of the construct on the surface. The fourth arm contains a chemically reactive maleimide group that provides covalent coupling with the cysteine of the $A\beta$-40 peptide. For the modification of the silicon substrate, T-silatrane was mixed with similar tetrahedral molecules containing silatrane in all arms. The use of the second molecule allowed us to decrease the surface density of active maleimide groups and hence the number of nonspecific events. The results of the contour length measurements for pH 5 and 2.7 are shown in Figure S5 of the Supporting Information. The distribution of the lengths is broad with a range from 10 to 45 nm. This is a range of contour lengths similar to that described above, given the fact that the contribution of the linkers to these values is ~10 nm.

■ DISCUSSION

Stability of Dimers of $A\beta$-40 and Molecular Mechanisms of Early Stages of Aggregation. The single-molecule force
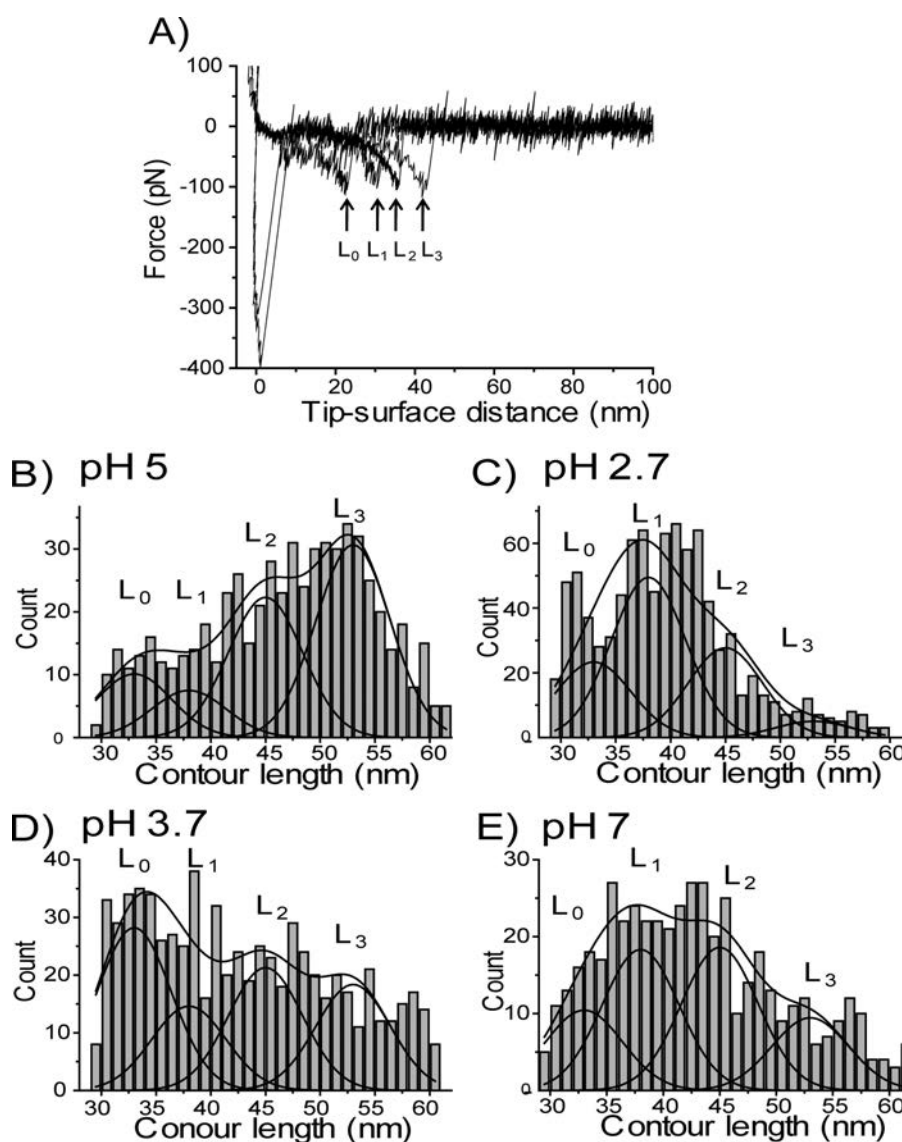
Figure 4. (A) Representative force curves for rupture events with different rupture lengths obtained at pH 5. All force curves were obtained at the same ALR regime (~34 nN/s) and correspond to rupture forces of ~120 pN. (B−E) Histograms of the contour length distributions measured at pH 5 (B), 2.7 (C), 3.7 (D), and 7 (E). Each histogram is approximated with four Gaussian curves with centers located around 33 (L_0), 38 (L_1), 45 (L_2), and 53 nm (L_3). The data were collected over the pulling rate range from 0.1 to 10 nN/s.

spectroscopy analysis revealed a number of novel properties of Aβ-40 in misfolded states. The DFS experiments demonstrate that the transiently formed dimers are characterized by lifetimes in the range of seconds, regardless of the pH. It is important to compare this value with the lifetime of misfolded conformations of the monomer peptides. When Aβ peptides are monomers, their conformational dynamics occurs in the range of 10^{-6}−10^{-9} s.[34] Some of these transient states existing on the nanosecond to microsecond time scale are misfolded conformations. When two misfolded monomers associate to form a dimer, their lifetime increases significantly, reaching a value of several seconds. Molecular dynamics (MD) simulations of the oligomeric structure of Aβ(25−35) revealed that dimerization and formation of stable β-sheet dimers takes place on the nanosecond time scale.[35] Furthermore, MD simulations of ologomeric Aβ-(17−42) showed that a double layer of β-hairpins is energetically favored.[36] Thus, the dimerization of misfolded proteins leads to

the stabilization of the misfolded states of Aβ peptides. However, the dimers show different properties depending on the pH. The DFS plot for pH 7 (Figure 3A) is represented by one line, yielding a profile of the energy landscape with one barrier (Figure 3B). The barrier height is $27.2k_BT$, which corresponds to a lifetime of 0.1 s. The dimer dissociation pathways under acidic conditions (pH 5, 3.7, and 2.7) are more complex because the DFS graphs have two slopes corresponding to two potential barriers in the energy landscapes. The inner barriers for these conditions have very close heights, corresponding to lifetimes in the range of 10 ms. The heights of outer barriers are larger and correspond to lifetimes over the range from 0.43 s (pH 3.7) to 2.7 s (pH 2.7).

Two major conclusions emerge from these findings. Compared to the monomeric proteins, the misfolded conformation of Aβ peptides in the dimeric state is 10^6 times more stable. This finding suggests that Aβ peptide dimers have a different
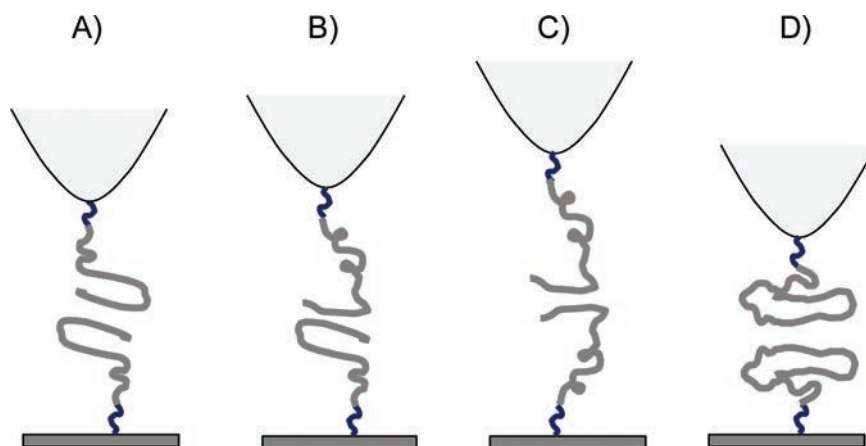
Figure 5. Schematics of four intermediate dimeric structures. (A) Dimer structure stabilized by the interaction between β-hairpins. (B) Dimer structure stabilized by the interaction between β-hairpins and the C-terminal segment of the peptide. (C) Dimer stabilized by the interaction of the C-terminal segments of the peptide. (D) Interaction between collapsed conformers of the Aβ-40 monomer.

conformation compared to that of the monomers. This is in agreement with the recent publication of Ono et al.,[4] in which a dramatic change in the secondary structure was observed between the monomer and dimer of photoinduced cross-linked Aβ-40. Although further oligomerizations increase the β-sheet content relative to the random coil content, these are gradual processes compared to that in the monomer to dimer transition. Given this conformational change preceding or along with dimerization,[4,37] our results suggest that the misfolded dimers have large lifetimes most likely through interactions with β-hairpins.

The increased stability of the dimers suggests the following mechanism for the aggregation process: Aβ peptides in the monomeric state are dynamic occurring on the nanosecond to microsecond time scale,[34,38] which allows Aβ to adopt various conformations, including misfolded states. When two monomers make a dimer, it remains in the misfolded state 10^6–10^9 times longer. Therefore, the probability of aggregation with the participation of dimers is 10^6–10^9 times higher compared to that with monomers. For example, the probability of the formation of tetramers with the assembly of two dimers will be 10^6 times higher compared to probability of the formation of trimers via the interaction of a dimer and a monomer. As a result, the preferred mechanism for aggregation is via dimers, rather than monomers. This assumption is in agreement with the recent publication of Bernstein et al.[3] Quantitative analysis using the ISI-MS method showed that oligomers with only even numbers of monomers, dimers, and tetramers for the Aβ-40 peptide are formed.

Additional support for the hypothesis of a critical role of Aβ peptide dimers in the aggregation kinetics is provided by recent publications.[4,39] These papers showed that stabilization of Aβ peptide dimers by cross-linking or mutation resulted in a rapid increase in the aggregation rate with a short lag phase. Additionally, a study[40] in which the hairpin conformation of Aβ peptide monomers was stabilized by intramolecular disulfide bonding demonstrated that the Aβ peptide oligomers assembled with stabilized β-sheets led to an increase in their toxicity compared to the control samples. Furthermore, Shankar et al. showed that Aβ dimers are the abundant species and have a high neurotoxicity through the analysis of the Aβ peptides isolated from brain.[12] This suggests an important biological role for Aβ dimers.

Structure of Misfolded Dimers. The measurements of the contour lengths (Figure 4A) provide insight into the structure of misfolded dimers of Aβ-40. Although the range of contour lengths is rather broad, the distribution is not smooth and can be divided into four groups, L_0, L_1, L_2, and L_3, as indicated in Figure 4B–E. In fibrils, Aβ chains interact with each other via β-hairpin structures; therefore, we assumed the presence of similar structures during probing experiments. The estimate for the contour length for this interaction produced the L_1 value. L_2 and L_3 correspond to hypothetical interactions of transiently opened hairpin structures. These are schematically shown in Figure 5. The model for the Aβ-40 dimer (Figure 5A) is assembled by two Aβ-40 molecules adopting the structure found in fibrils. Once again, monomers interact via the β-hairpin and residues D1–Y10 of the N-terminus are nonstructured. The rupture of such a dimer should occur with a contour length of 38 ± 4 nm, which includes the length of the linkers (26 ± 4 nm) and unstructured N-terminal segments of the peptides (7–8 nm)[41] and two hairpin structures (~ 4 nm).[29] The overall length correlates very well with the L_1 value in Figure 4B–E. Figure 5B shows the model in which the dimer is formed by the Aβ-40 peptides in two different conformations. One conformation is the monomer with a hairpin structure that interacts with the C-terminal segment of a second Aβ-40, which is half of the hairpin structure. The rupture of this construct occurs at contour lengths of 45 ± 4 nm, which is larger compared to the previous model due to the extended length of the N-terminal segment in one of the constructs. This overall length is in agreement with the L_2 value. Similarly, the model in Figure 5C corresponds to the assembly of two Aβ-40 molecules through their C-terminal regions with extended unstructured N-terminal regions contributing ~ 23 nm to the contour lengths of the linkers (26 ± 4 nm). The overall expected contour length for the rupture of such a construct is 53 ± 4 nm, which is close to L_3.

To explain the appearance of rupture events with lengths as short as L_0, we hypothesize that the dimers can adopt a collapsed conformation in which residues A2–F4 of the N-terminal region are involved in the stabilization of the dimer. Such a model is supported by molecular dynamics simulation[34] showing that N-terminal residues of Aβ-40 are involved in the formation of oligomers. This, however, is in disagreement with the work of Takeda et al.[42] The structure of the dimer with interactions

between collapsed structures is sketched schematically in Figure 5D. The rupture of such a dimer occurs after stretching of linkers, providing the expected contour length of 33 ± 4 nm, which is close to the L_0 value.

It is important to apply this model to understanding the effect of pH on the conformation of Aβ dimers. The data shown in Figure 4B indicate that at pH 5, conformers L_2 and L_3 are the most predominant species, suggesting that under these conditions the stabilization of dimers by models B and C is rather favorable. In contrast, at pH 2.7 (Figure 4C) complexes A and B comprise the most preferable states for the dimers with a few events with conformation C. This difference can be explained by electrostatic repulsion that is stronger at acidic pH than at pH 5, which is close to the pI value for Aβ-40.

Additional insight into the structure of the transiently formed dimers is provided by the values of the rupture forces. The rupture forces of Aβ-40 dimers were in the range of 60—100 pN at loading rates of 4—20 nN/s (200 nm $\sim$ 1 μm/s) at pH 7. We can compare this value with the data for the AFM unfolding of titin Ig domains that mainly consist of β-sheet structures.[43] The unfolding forces obtained over the loading rate range of 200—400 nm/s were 170—180 pN, which is $\sim$3 times larger ($\sim$60 pN) than the rupture force for Aβ-40 obtained at the same loading rate. At the same time, unfolding of α-helical structure of T4 lysozyme required considerably less force, $\sim$60 pN compared to $\sim$100 pN for Aβ-40, at a loading rate of 1 μm/s.[44] This comparison suggests that the conformation of Aβ-40 dimers is less stable than β-sheets but more stable than α-helical structures. This conclusion is in agreement with the structural analysis of Aβ-40[4,6] and suggests that unstructured monomers undergo significant conformational changes while they are oligomerized.

Altogether, AFM force spectroscopy identified long lifetimes of misfolded Aβ-40 dimers, compared to the monomers that retain their misfolded state for very short periods of time. Additionally, the misfolded dimers are 10^6 times more stable. Note that qualitatively similar results for lifetimes were obtained previously from α-synuclein.[19,20,26] Thus, the long lifetime of the Aβ-40 dimers is a fundamental property of this peptide and possible for other amyloidogeneic proteins. On the basis of these findings, we propose a model in which the formation of dimers is a mechanism by which aggregation prone misfolded proteins become highly stabilized. Because of its long lifetime, the probability that the dimer will have further interactions dramatically increases. Thus, the ability to form long-lived dimers is a fundamental property of misfolded proteins and triggers the protein aggregation process. This is an entirely novel view of the aggregation process that may lead to a paradigm shift in the development of diagnostic and therapeutic treatments for protein misfolding diseases, narrowing the search to approaches that can prevent dimer formation. Given the ability of AFM to detect the interaction between the proteins at the single-molecule level, AFM force spectroscopy may be a potential diagnostic and therapeutic tool in the future. AFM in imaging mode is a primary tool for the visualization of amyloid aggregates,[45] so the combination of both AFM capabilities would provide important information about the mechanism of the aggregation process. However, the small size of monomeric Aβ peptides complicates unambiguous identification of all oligomeric species in the AFM scans. Further improvement in the AFM imaging methodology is needed to accomplish this goal.

■ ASSOCIATED CONTENT

ⓢ Supporting Information. Details of the synthesis of cysteine-modified Aβ-40 and the tetrahedrally shaped tripodal silatrane (T-shaped) molecule, contour length distribution measured with the use of the T-silatrane molecules, and estimates of the polydispersity of the linker molecule. This material is available free of charge via the Internet at http://pubs.acs.org.

■ AUTHOR INFORMATION

Corresponding Author
*Department of Pharmaceutical Sciences, University of Nebraska Medical Center, Omaha, NE 68198. Phone: (402) 559-1971. Fax: (402) 559-9543. E-mail: ylyubchenko@unmc.edu.

■ ACKNOWLEDGMENT

■ ABBREVIATIONS

AFM, atomic force microscopy; ALR, apparent loading rate; Aβ, amyloid β; APS, 1-(3-aminopropyl)silatrane; α-Syn, α-synuclein; DFS, dynamic force spectroscopy; FDC, force—distance curve; MAS, maleimide silatrane; PEG, polyethylene glycol; TCEP, tris(2-carboxyethyl)phosphine; T-silatrane, tetrahedrally shaped tripodal silatrane molecule; WLC, wormlike chain.

■ REFERENCES

(1) Dobson, C. M. (2003) Protein folding and misfolding. *Nature* 426, 884–890.

(2) Bucciantini, M., Giannoni, E., Chiti, F., Baroni, F., Formigli, L., Zurdo, J., Taddei, N., Ramponi, G., Dobson, C. M., and Stefani, M. (2002) Inherent toxicity of aggregates implies a common mechanism for protein misfolding diseases. *Nature* 416, 507–511.

(3) Bernstein, S. L., Dupuis, N. F., Lazo, N. D., Wyttenbach, T., Condron, M. M., Bitan, G., Teplow, D. B., Shea, J.-E., Ruotolo, B. T., Robinson, C. V., and Bowers, M. T. (2009) Amyloid-β protein oligomerization and the importance of tetramers and dodecamers in the aetiology of Alzheimer's disease. *Nat. Chem.* 1, 326–331.

(4) Ono, K., Condron, M. M., and Teplow, D. B. (2009) Structure-neurotoxicity relationships of amyloid β-protein oligomers. *Proc. Natl. Acad. Sci. U.S.A.* 106, 14745–14750.

(5) Paravastu, A. K., Leapman, R. D., Yau, W. M., and Tycko, R. (2008) Molecular structural basis for polymorphism in Alzheimer's β-amyloid fibrils. *Proc. Natl. Acad. Sci. U.S.A.* 105, 18349–18354.

(6) Chimon, S., Shaibat, M. A., Jones, C. R., Calero, D. C., Aizezi, B., and Ishii, Y. (2007) Evidence of fibril-like β-sheet structures in a neurotoxic amyloid intermediate of Alzheimer's β-amyloid. *Nat. Struct. Mol. Biol.* 14, 1157–1164.

(7) Kim, J., and Lee, M. (2004) Observation of multi-step conformation switching in β-amyloid peptide aggregation by fluorescence resonance energy transfer. *Biochem. Biophys. Res. Commun.* 316, 393–397.

(8) Hofrichter, J., Ross, P. D., and Eaton, W. A. (1974) Kinetics and mechanism of deoxyhemoglobin S gelation: A new approach to understanding sickle cell disease. *Proc. Natl. Acad. Sci. U.S.A. 71*, 4864–4868.

(9) Jarrett, J. T., and Lansbury, P. T., Jr. (1993) Seeding "one-dimensional crystallization" of amyloid: A pathogenic mechanism in Alzheimer's disease and scrapie? *Cell 73*, 1055–1058.

(10) Meyer-Luehmann, M., Spires-Jones, T. L., Prada, C., Garcia-Alloza, M., de Calignon, A., Rozkalne, A., Koenigsknecht-Talboo, J., Holtzman, D. M., Bacskai, B. J., and Hyman, B. T. (2008) Rapid appearance and local toxicity of amyloid-β plaques in a mouse model of Alzheimer's disease. *Nature 451*, 720–724.

(11) Deshpande, A., Mina, E., Glabe, C., and Busciglio, J. (2006) Different conformations of amyloid β induce neurotoxicity by distinct mechanisms in human cortical neurons. *J. Neurosci. 26*, 6011–6018.

(12) Shankar, G. M., Li, S., Mehta, T. H., Garcia-Munoz, A., Shepardson, N. E., Smith, I., Brett, F. M., Farrell, M. A., Rowan, M. J., Lemere, C. A., Regan, C. M., Walsh, D. M., Sabatini, B. L., and Selkoe, D. J. (2008) Amyloid-β protein dimers isolated directly from Alzheimer's brains impair synaptic plasticity and memory. *Nat. Med. 14*, 837–842.

(13) Kirkitadze, M. D., Bitan, G., and Teplow, D. B. (2002) Paradigm shifts in Alzheimer's disease and other neurodegenerative disorders: The emerging role of oligomeric assemblies. *J. Neurosci. Res. 69*, 567–577.

(14) Bitan, G., and Teplow, D. B. (2004) Rapid photochemical cross-linking: A new tool for studies of metastable, amyloidogenic protein assemblies. *Acc. Chem. Res. 37*, 357–364.

(15) He, X., Giurleo, J. T., and Talaga, D. S. (2009) Role of small oligomers on the amyloidogenic aggregation free-energy landscape. *J. Mol. Biol. 395*, 134–154.

(16) McAllister, C., Karymov, M. A., Kawano, Y., Lushnikov, A. Y., Mikheikin, A., Uversky, V. N., and Lyubchenko, Y. L. (2005) Protein interactions and misfolding analyzed by AFM force spectroscopy. *J. Mol. Biol. 354*, 1028–1042.

(17) Lyubchenko, Y. L., Sherman, S., Shlyakhtenko, L. S., and Uversky, V. N. (2006) Nanoimaging for protein misfolding and related diseases. *J. Cell. Biochem. 99*, 52–70.

(18) Kransnoslobodtsev, A. V., Shlyakhtenko, L. S., Ukraintsev, E., Zaikova, T. O., Keana, J. F., and Lyubchenko, Y. L. (2005) Nanomedicine and protein misfolding diseases. *Nanomedicine 1*, 300–305.

(19) Yu, J., and Lyubchenko, Y. L. (2009) Early stages for Parkinson's development: α-Synuclein misfolding and aggregation. *J. Neuroimmune Pharmacol. 4*, 10–16.

(20) Yu, J., Malkova, S., and Lyubchenko, Y. L. (2008) α-Synuclein misfolding: Single molecule AFM force spectroscopy study. *J. Mol. Biol. 384*, 992–1001.

(21) Khandogin, J., and Brooks, C. L., III (2007) Linking folding with aggregation in Alzheimer's β-amyloid peptides. *Proc. Natl. Acad. Sci. U.S.A. 104*, 16880–16885.

(22) Valerio, M., Porcelli, F., Zbilut, J. P., Giuliani, A., Manetti, C., and Conti, F. (2008) pH effects on the conformational preferences of amyloid β-peptide (1−40) in HFIP aqueous solution by NMR spectroscopy. *ChemMedChem 3*, 833–843.

(23) Coles, M., Bicknell, W., Watson, A. A., Fairlie, D. P., and Craik, D. J. (1998) Solution structure of amyloid β-peptide(1−40) in a water-micelle environment. Is the membrane-spanning domain where we think it is? *Biochemistry 37*, 11064–11077.

(24) Ryuta, J., Morita, E., Tanaka, T., and Shimanuki, Y. (1990) Crystal-Originated Singularities on Si Wafer Surface after Sc1 Cleaning. *Jpn. J. Appl. Phys. 2* (29), L1947–L1949.

(25) Bustamante, C., Marko, J. F., Siggia, E. D., and Smith, S. (1994) Entropic elasticity of λ-phage DNA. *Science 265*, 1599–1600.

(26) Yu, J., Warnke, J., and Lyubchenko, Y. L. (2011) Nanoprobing of α-synuclein misfolding and aggregation with atomic force microscopy. *Nanomedicine 7*, 146–152.

(27) Krasnoslobodtsev, A. V., Shlyakhtenko, L. S., and Lyubchenko, Y. L. (2007) Probing interactions within the synaptic DNA-SfiI complex by AFM force spectroscopy. *J. Mol. Biol. 365*, 1407–1416.

(28) Tinoco, I., Jr., and Bustamante, C. (2002) The effect of force on thermodynamics and kinetics of single molecule reactions. *Biophys. Chem. 101−102*, 513–533.

(29) Petkova, A. T., Yau, W. M., and Tycko, R. (2006) Experimental constraints on quaternary structure in Alzheimer's β-amyloid fibrils. *Biochemistry 45*, 498–512.

(30) Petkova, A. T., Ishii, Y., Balbach, J. J., Antzutkin, O. N., Leapman, R. D., Delaglio, F., and Tycko, R. (2002) A structural model for Alzheimer's β-amyloid fibrils based on experimental constraints from solid state NMR. *Proc. Natl. Acad. Sci. U.S.A. 99*, 16742–16747.

(31) Lyubchenko, Y. L., Kim, B. H., Krasnoslobodtsev, A. V., and Yu, J. (2010) Nanoimaging for protein misfolding diseases. *Wiley Interdisciplinary Reviews of Nanomedicine and Nanobiotechnology 2*, 526–543.

(32) Evans, E. (2001) Probing the relation between force—lifetime —and chemistry in single molecular bonds. *Annu. Rev. Biophys. Biomol. Struct. 30*, 105–128.

(33) Bell, G. I. (1978) Models for the specific adhesion of cells to cells. *Science 200*, 618–627.

(34) Urbanc, B., Betnel, M., Cruz, L., Bitan, G., and Teplow, D. B. (2010) Elucidation of amyloid β-protein oligomerization mechanisms: Discrete molecular dynamics study. *J. Am. Chem. Soc. 132*, 4266–4280.

(35) Wei, G., Jewett, A. I., and Shea, J. E. (2010) Structural diversity of dimers of the Alzheimer amyloid-β(25−35) peptide and polymorphism of the resulting fibrils. *Phys. Chem. Chem. Phys. 12*, 3622–3629.

(36) Miller, Y., Ma, B., and Nussinov, R. (2009) Polymorphism of Alzheimer's Aβ17−42 (p3) oligomers: The importance of the turn location and its conformation. *Biophys. J. 97*, 1168–1177.

(37) Kumar, S., and Udgaonkar, J. B. (2009) Conformational conversion may precede or follow aggregate elongation on alternative pathways of amyloid protofibril formation. *J. Mol. Biol. 385*, 1266–1276.

(38) Kim, S., Takeda, T., and Klimov, D. K. (2010) Mapping conformational ensembles of Aβ oligomers in molecular dynamics simulations. *Biophys. J. 99*, 1949–1958.

(39) Yamaguchi, T., Yagi, H., Goto, Y., Matsuzaki, K., and Hoshino, M. (2010) A disulfide-linked amyloid-β peptide dimer forms a proto-fibril-like oligomer through a distinct pathway from amyloid fibril formation. *Biochemistry 49*, 7100–7107.

(40) Sandberg, A., Luheshi, L. M., Sollvander, S., Pereira de Barros, T., Macao, B., Knowles, T. P., Biverstal, H., Lendel, C., Ekholm-Petterson, F., Dubnovitsky, A., Lannfelt, L., Dobson, C. M., and Hard, T. (2010) Stabilization of neurotoxic Alzheimer amyloid-β oligomers by protein engineering. *Proc. Natl. Acad. Sci. U.S.A. 107*, 15595–15600.

(41) Ainavarapu, S. R., Brujic, J., Huang, H. H., Wiita, A. P., Lu, H., Li, L., Walther, K. A., Carrion-Vazquez, M., Li, H., and Fernandez, J. M. (2007) Contour length and refolding rate of a small protein controlled by engineered disulfide bonds. *Biophys. J. 92*, 225–233.

(42) Takeda, T., and Klimov, D. K. (2009) Probing the effect of amino-terminal truncation for Aβ1−40 peptides. *J. Phys. Chem. B 113*, 6692–6702.

(43) Rief, M., Gautel, M., Oesterhelt, F., Fernandez, J. M., and Gaub, H. E. (1997) Reversible unfolding of individual titin immunoglobulin domains by AFM. *Science 276*, 1109–1112.

(44) Yang, G., Cecconi, C., Baase, W. A., Vetter, I. R., Breyer, W. A., Haack, J. A., Matthews, B. W., Dahlquist, F. W., and Bustamante, C. (2000) Solid-state synthesis and mechanical unfolding of polymers of T4 lysozyme. *Proc. Natl. Acad. Sci. U.S.A. 97*, 139–144.

(45) Stine, W. B., Jr., Dahlgren, K. N., Krafft, G. A., and LaDu, M. J. (2003) In vitro characterization of conditions for amyloid-β peptide oligomerization and fibrillogenesis. *J. Biol. Chem. 278*, 11612–11622.